

INTRODUCTION TO WAVEFRONT CODING FOR INCOHERENT IMAGING

M. Roche¹

Abstract. We propose in this paper an introduction to the wavefront coding technique for incoherent imaging. Wavefront coding introduces image processing in the conception of an imaging system. It consists in introducing controlled aberrations in the optics able to reduce, after processing, some defaults of the optical system such as defocus, chromaticity. We present the basis of wavefront coding and illustrate them on two images with different characteristics: a spoke pattern and a galaxy image.

1 Introduction

In traditional imaging systems, the design of the optics and the processing of the recorded images are two separate steps. High aperture instruments allow one to obtain images with high resolution, with high signal to noise ratio due to the large amount of light collected and high depth of field. However these instruments are more subject to aberrations like defocus as instrument with smaller aperture size.

In hybrid imaging systems, optics and processing are considered jointly and designed together. These last imaging systems allow one to use optics of lower quality and thus with reduced cost, the quality of the images warranted not by the quality of the optics but by the processing step. A good example of the interest to associate the image processing to the optics could be the Hubble Space Telescope (HST). It was launched in early 1990, at that time a spherical aberration has been detected, leading to a blurring of the images. The first simple and effective way to solve this degradation was to introduce image processing. Latter in 1993, this default has been corrected by introducing the COSTAR corrective optics in a Shuttle mission.

Wavefront coding was introduced by Dowski & Cathey (1995) for incoherent imaging. They propose to introduce a phase mask in the imaging system, designed

¹ Centrale Marseille, CNRS, Aix-Marseille Université, Fresnel, UMR 7249,
13013 Marseille, France

to make the Point Spread Function (PSF) of the instrument insensitive to some aberrations such as chromaticity, or spherical aberrations. It is also used to enhance the depth of field of an instrument by making the imaging system insensitive to defocus aberrations.

Wavefront coding is now used in many domains such as security for iris recognition (Narayanswamy *et al.* 2004) where it is useful for capturing an iris without active user cooperation, thermal imagery (Muyo *et al.* 2004) for controlling thermally induced defocus aberrations in infrared imaging system, fluorescence microscopy (Arnison *et al.* 2007) to increase the depth of field. In astronomy, wavefront coding has been not yet used but it has been shown (Kubala *et al.* 2004) that as telescope performances are limited by aberrations, misalignment, temperature related defaults, this technique will provide improvement of the quality of the images.

This article is an introduction to wavefront coding technique. It does not contain new results on it but presents the different steps that lead, from a degraded image, to an image of higher quality after a post-processing. For the sake of clarity and conciseness, the paper only discuss about defocus default and on the use of a cubic phase mask.

It is organized as follows. In Section 2, the principle of image formation in a classical imaging system is presented. In Section 3, a default of defocus in the optics is introduced and modeled. In Section 4, the wavefront coding is detailed and results are presented on two different images using a cubic phase mask. Section 5 presents the optimization of the parameter of the cubic phase mask. Finally Section 6 discusses on the robustness of wavefront coding in presence of defocus.

2 Image formation in coherent and incoherent imaging

The wavefront coding technique is developed for incoherent illumination. In the following, we first discuss about the coherent illumination of an object, which is needed to explain the incoherent case.

2.1 Image of a point like object

Let us assume that we observe with an optical instrument a point like source, that can be modeled by a Dirac distribution $\delta(x, y)$. When the imaging system is only limited by diffraction, the image amplitude of this point-like source is given by the Fraunhofer diffraction pattern of the exit pupil of the imaging system²

$$H(x, y) = \frac{A}{\lambda L} \widehat{P} \left(\frac{x}{\lambda L}, \frac{y}{\lambda L} \right) \quad (2.1)$$

where A is a constant amplitude traducing the attenuation of the amplitude by the imaging system, λ is the wavelength of the light emitted by a point like object,

²For detailed calculus see for example Goodman (2005), chapter 6.

L is the distance between the exit pupil and the image plane, \hat{P} is the Fourier transform of the pupil aperture, x and y the coordinates in the plane of the exit pupil.

In the case of a circular pupil, $H(x, y)$ corresponds to the Airy function of the instrument. For notational convenience, we will assume in the following that $\frac{A}{\lambda L}$ and λL equal unity.

2.2 Impulse function for the observation of an entire object

2.2.1 Coherent illumination

When coherent illumination is considered, all the point of the object emit field whose phasor amplitude vary in unison. Thus the image of the object is obtained by summing all the contributions of the complex amplitude coming from all the point of the object. A coherent imaging system is thus linear in complex amplitude. Assuming that one point of the object is modeled by a Dirac distribution δ_i , it can be shown³ that the received amplitude from the object is given by:

$$A(x, y) = \sum_i (\delta_i \otimes H)(x, y) = ((\sum_i \delta_i) \otimes H)(x, y) \quad (2.2)$$

where \otimes represents the convolution product, $H(x, y)$ is called the amplitude PSF of the instrument. This can be rewritten:

$$A(x, y) = (O \otimes H)(x, y) \quad (2.3)$$

with $O = \sum_i \delta_i$ the amplitude of the object. The Fourier transform of the amplitude PSF is called the Amplitude Coherent Transfert Function (ACTF). In the case of a symmetric pupil (almost the cases encountered), it is easy to show that:

$$ACTF(\mu, \nu) = P(\mu, \nu) \quad (2.4)$$

with P the pupil of the instrument, μ, ν the coordinates in the frequency plane.

For a circular aperture of diameter d in coherent illumination, the instrument behaves as a low-pass filter with cutting frequency $\frac{d}{2}$.

In general, the optic instruments measure intensity that means

$$i(x, y) = |A(x, y)|^2 = |O \otimes H|^2(x, y). \quad (2.5)$$

2.2.2 Incoherent illumination

In the case of incoherent illumination, the phasor amplitudes are totally uncorrelated, the complex amplitude can no more be added. In this case, it can be shown⁴ that an incoherent imaging system is linear in intensity:

$$i(x, y) = (o \otimes G)(x, y) \quad (2.6)$$

³For detailed calculus see for example Goodman (2005), chapter 6.

⁴See for example Goodman (2005) for detailed calculus, chapter 6.

where $G(x, y) = |H(x, y)|^2$, $i(x, y)$ the intensity of the image observed and $o(x, y)$ the intensity of the object.

$|H(x, y)|^2$ represents the intensity point spread function of the instrument, it will be denoted PSF in the following. The Fourier transform of this PSF is called the Optical Transfer Function (OTF) and its modulus the Modulated Transfer Function (MTF).

3 Analysis of the influence of defocus

Let us assume an incoherent imaging system with a circular pupil $P(\mu, \nu)$ of diameter d , that presents a focus default that is spatially constant over the pupil. This defocus can be modeled in the pupil plane by introducing a supplementary phase:

$$e^{i\Psi_\lambda(\nu^2+\mu^2)} \quad (3.1)$$

where e^a represents the exponential function of a , Ψ_λ corresponds to the defocalisation parameter and $i = \sqrt{-1}$. Ψ_λ depends on the diameter of the pupil d , on the distance between the object and the primary plane of the lens d_0 , on the distance between the secondary plane of the lens and the CCD camera d_{ccd} and on the focal distance of the lens $f(\lambda)$ (Dowski *et al.* 1995)

$$\Psi_\lambda = \frac{\pi d^2}{4\lambda} \left(\frac{1}{f(\lambda)} - \frac{1}{d_0} - \frac{1}{d_{ccd}} \right) = \frac{2\pi}{\lambda} W_{20} \quad (3.2)$$

with W_{20} is the traditional defocus aberration constant. The pupil of the imaging system in presence of defocus is thus:

$$P'(\nu, \mu) = P(\nu, \mu) e^{i\Psi_\lambda(\nu^2+\mu^2)}. \quad (3.3)$$

From Equation (2.1), the PSF of this imaging system in the case of incoherent imaging is given by:

$$|H(x, y)|^2 = \left| \widehat{P'}(x, y) \right|^2. \quad (3.4)$$

Figure 1 shows respectively the PSF and the MTF for an instrument of circular aperture when no defocus default is presents a) and c), and when a defocus of parameter $\Psi_{\lambda_3} = 50$ is introduced b) d). The defocus induces a PSF extended with respect to the ideal one (a) and consequently a MTF with an important reduction of the high frequencies. The defocus will introduce a blurring effect in the imaged object.

Figure 2 represents a central cut of the MTF in the case of incoherent imaging system with a circular pupil in presence of different defocus. Three different defocus are considered with $\Psi_{\lambda_1} < \Psi_{\lambda_2} < \Psi_{\lambda_3}$. The circular pupil behaves as a low-pass filter, an increase of the parameter of defocus implies a reduction of the cut-off frequency and introduces oscillations in the MTF with apparition of zeros.

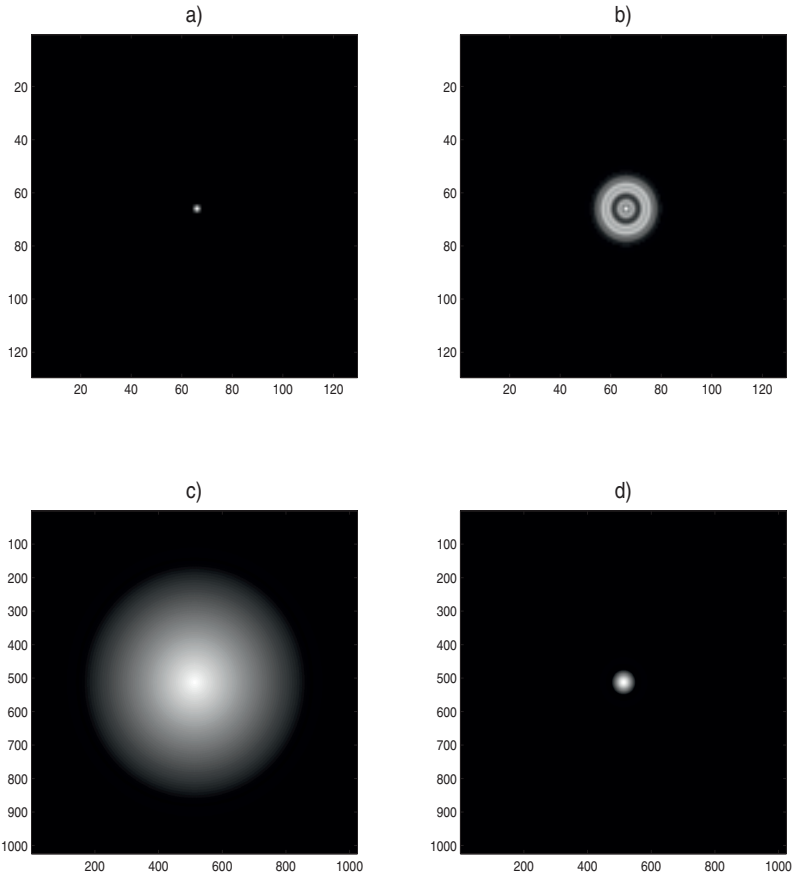


Fig. 1. Representation of the PSF (first line) and MTF (second line) of an instrument with circular aperture when in focus a), c) and when a defocus of parameter $\Psi_{\lambda_3} = 50$ is introduced b), d). In order to improve the visualization, figures a) and b) correspond to a central part of size 128×128 of the entire PSF (of size 1024×1024).

The effect of the MTF on two different imaged object is obtained from 2.6. The two object considered are respectively, a spoke pattern with high spatial frequencies, and the galaxie UGC 1810 taken by the Hubble Space Telescope⁵ containing mostly low spatial frequencies. The results are presented in Figures 3 and 4 which shows the blurring effect appearing in the observed image when the imaging system presents a defocus default of parameter $\Psi_{\lambda_3} = 50$. This blurring effect appears essentially on the edge and on the center of the spoke pattern (Fig. 3c) whereas it is visible in the entire image of the galaxy (Fig. 4c) leading to the disappearance of the stars (point like object).

⁵<http://hubblesite.org/gallery/album/galaxy/hires/true/>

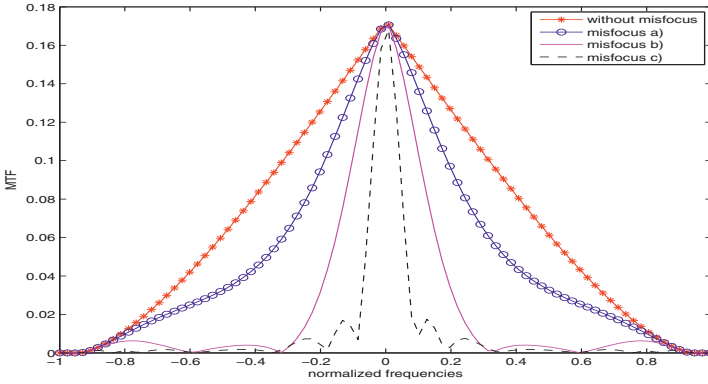


Fig. 2. Effect of different defocus (with a) $\Psi_{\lambda_1} = 10$, b) $\Psi_{\lambda_2} = 20$, c) $\Psi_{\lambda_3} = 50$) on the Modulated Transfer Function (MTF) of an incoherent imaging system with a circular aperture as a function of normalized frequencies (the maximum frequency equals one).

4 Correction of the defocus

The observed image (Figs. 3c and 4c) can be processed to reduce the effect of the PSF on the observation. If the PSF is known, classical deconvolution techniques can be implemented allowing to reconstruct an object closed to the true one (Figs. 3a and 4a) (when no noise is present⁶) to obtain the reconstructed image of Figures 3d and 4d. When a defocus is introduced (Figs. 3c and 4c), the image is blurred. The blurring effect can be suppressed if it is known (Figs. 3e and 4e). However in most cases this default is not known leading to deconvolved image of Figures 3f and 4f. In these cases, it is evident that the blurring effect has been neither suppressed nor reduced with respect to Figures 3c and 4c.

4.1 Introduction of wavefront coding

The wavefront coding was introduced in Dowski & Cathey (1995). It consists in introducing a phase mask in the pupil. This phase mask is introduced in order to correct the defaults of the imaging system: sphericity, chromatic aberrations (Wach *et al.* 1998), defocus... Moreover, this mask is constructed to avoid the presence of zeros in the corresponding PSF allowing first to preserve frequencies, and to avoid calculus errors in the deconvolution process.

In the pupil plane, the mask can be modeled by:

$$M(\nu, \mu) = e^{i\Phi(\nu, \mu)} \quad (4.1)$$

where $\Phi(\nu, \mu)$ characterizes the shape of the mask, $|\nu| < 1$ and $|\mu| < 1$ are the normalized frequency coordinates.

⁶Of course this hypothesis is not realist but allows to simplify the problem and to present basis on image formation.

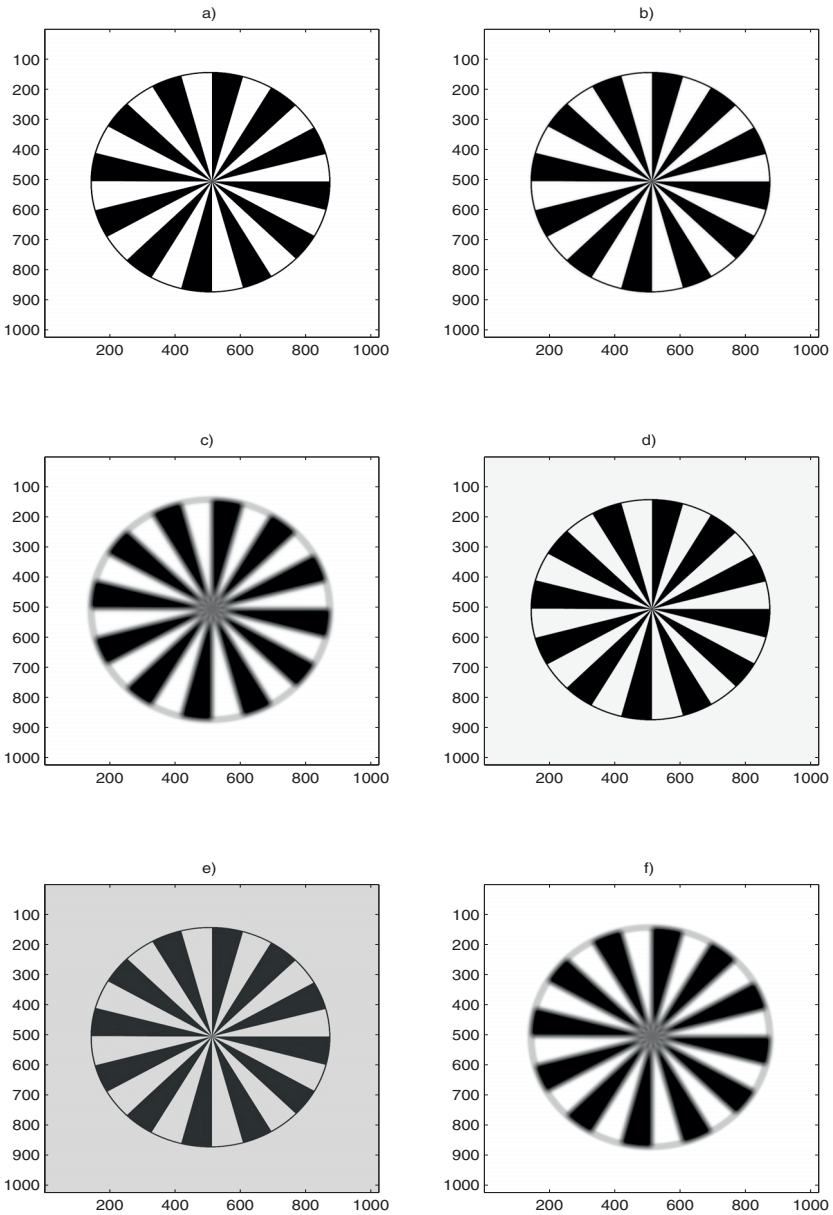


Fig. 3. Effect of different degradation on the initial object a): b) with an ideal circular pupil with a diameter of 480 pixels, c) with a defocus of $\Psi_{\lambda_3} = 50$ on the observation. Deconvolution of the observed image: d) deconvolution of b), e) deconvolution of c) with the defocus known, f) deconvolution of c) with the defocus unknown.

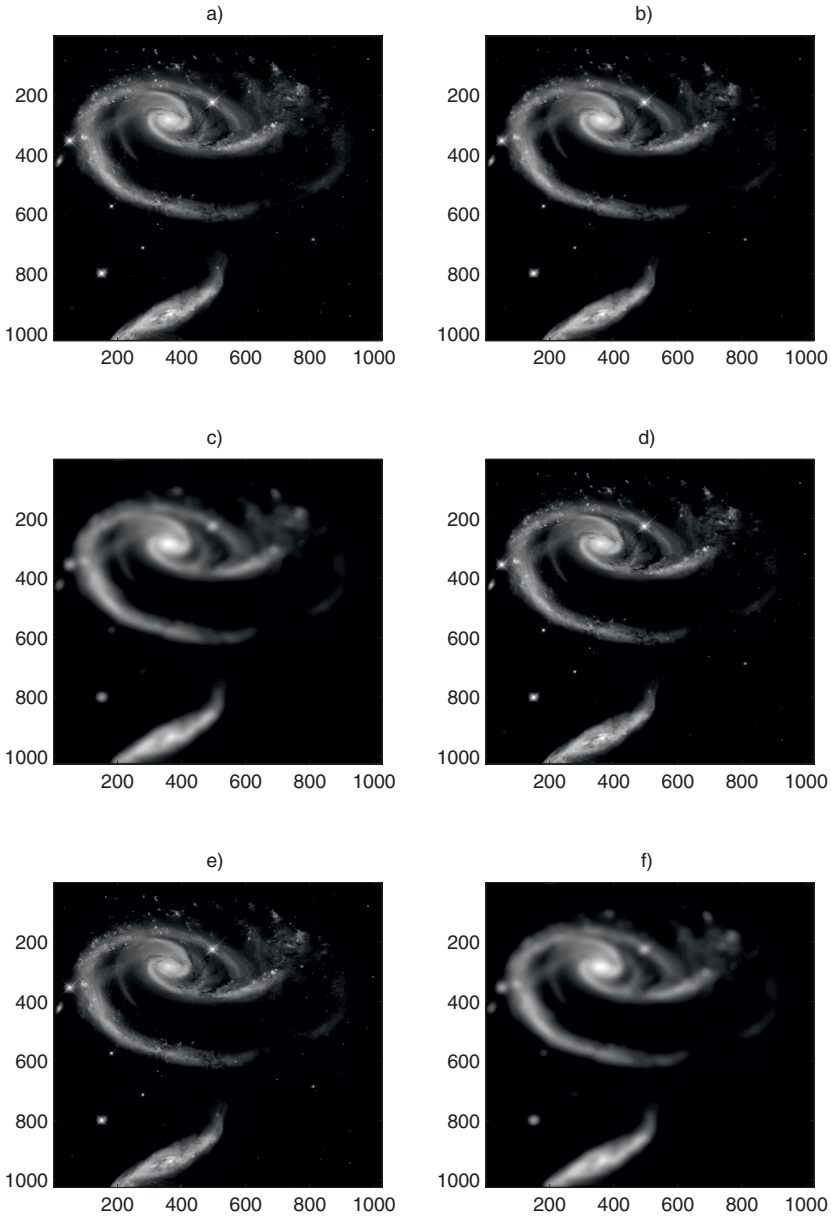


Fig. 4. Effect of different degradation on the initial object a): b) with an ideal circular pupil with a diameter of 480 pixels, c) with a defocus of $\Psi_{\lambda_3} = 50$ on the observation. Deconvolution of the observed image: d) deconvolution of b), e) deconvolution of c) with the defocus known, f) deconvolution of c) with the defocus unknown.

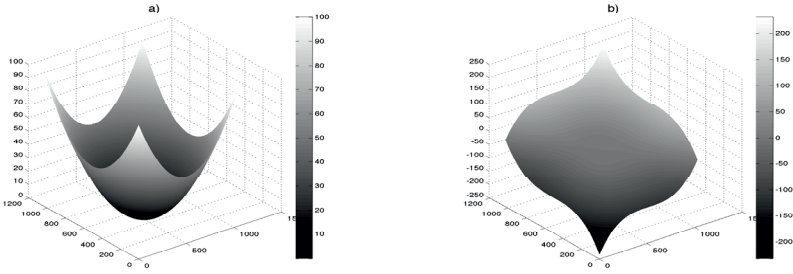


Fig. 5. Representation of the phases of a) the defocus default of parameter $\Psi_{\lambda_3} = 50$ and b) the phase introduced with a cubic phase mask of parameter $\alpha = 116$.

Wavefront coding leads in presence of defocus to a new pupil

$$P_c(\nu, \mu) = P'(\nu, \mu) \cdot M(\nu, \mu) = P(\nu, \mu) e^{i\Psi_\lambda(\nu^2 + \mu^2)} e^{i\Phi(\nu, \mu)}. \quad (4.2)$$

We focus in this paper on wavefront coding used to increase the depth of field, leading to optical system insensitive to defocus. Different phase mask have been proposed in the litterature to increase the depth of field: cubic phase mask (Dowski *et al.* 1995), logarithmic (Sherif *et al.* 2004; Zhao *et al.* 2008), fractionnal-power (Sauceda *et al.* 2004), exponentiel (Yang *et al.* 2007), polynomial (Caron *et al.* 2008), asymmetric phase mask (Castro *et al.* 2004) and have been compared (Diaz *et al.* 2010; Sherif *et al.* 2004; Yang *et al.* 2007) with respect to different criterion depending on the the aimed application.

These different phase masks are obtained by consideration of different criterion. In Neil *et al.* (2000), an optimization is done to obtain a particular form for the final PSF in the case of confocal microscope. In S. Prasad *et al.* (2004), the authors use the Fisher information and the Strehl ratio to find the mask that reduces the sensitivity of the phase to misfocus.

The cubic phase mask, we consider in the following, proposed by Dowski *et al.* (1995), was obtained by using the ambiguity function and the stationary-phase method.

Let us consider a cubic phase mask of the form

$$\Phi(\nu, \mu) = \alpha(\nu^3 + \mu^3). \quad (4.3)$$

Figure 5 illustrates the phases of a defocus default of parameter $\Psi_{\lambda_3} = 50$ and the phase introduced with a cubic phase mask of parameter $\alpha = 116$.

This mask was constructed to minimize the variation of the OTF with defocus. It presents only one parameter to optimize (α) with respect to the application, leading to a simple mask. Other masks introducing more parameters lead to better results in general, but increase the complexity of the mask.

Figure 6 represents respectively the PSF and the MTF of an instrument with circular aperture with a cubic phase mask of parameter $\alpha = 116$ when no defocus

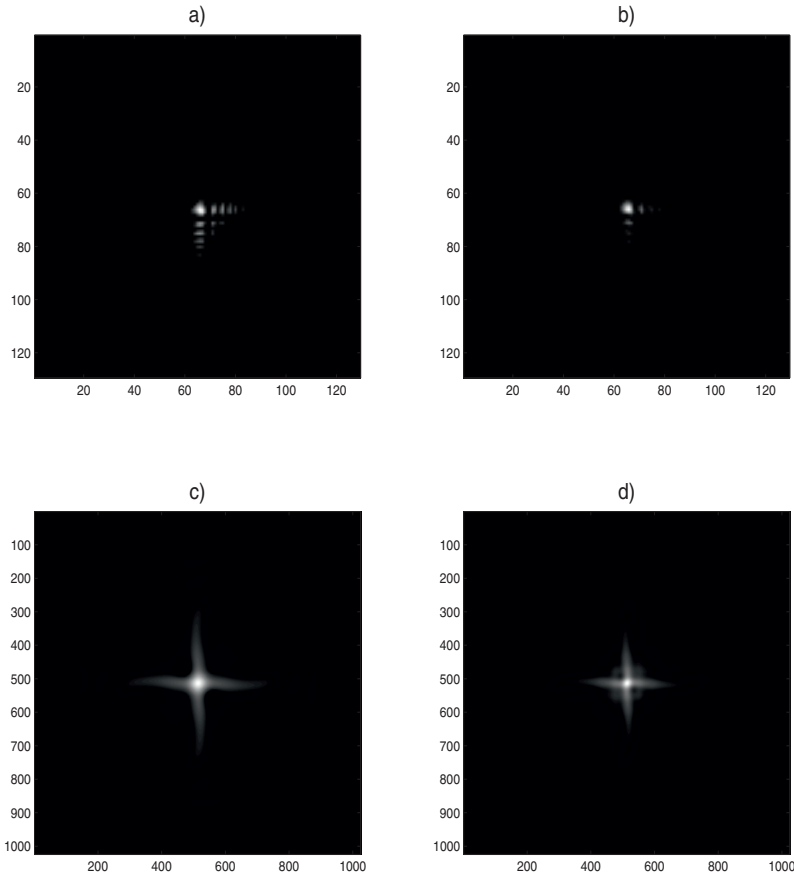


Fig. 6. Representation of the PSF (first line) and MTF (second line) of an instrument with circular aperture with a cubic phase mask of parameter $\alpha = 116$ when no defocus default is present a) c) and when a defocus of parameter $\Psi_{\lambda_3} = 50$ is introduced b) d). In order to improve the visualization, Figures a) and b) correspond to a central part of size 128×128 of the entire PSF (of size 1024×1024).

default is present a), c) and when a defocus of parameter $\Psi_{\lambda_3} = 50$ is introduced b), d). The wavefront coding leads to small noticeable changes in the PSF and in the MTF with defocus.

Figure 7 shows a central cut of the MTFs of Figures 1c, d and 6c, d, representative of different configurations: imaging system with no default, imaging system with defocus default of parameter $\Psi_{\lambda_3} = 50$, imaging system with wavefront coding when no defocus aberration exists and in presence of defocus. A cubic phase mask is used with parameter $\alpha = 116$. The use of wavefront coding allows to increase the cut-off frequency and to reduce the number of zeros. Moreover, the amplitude of the MTF is increased.

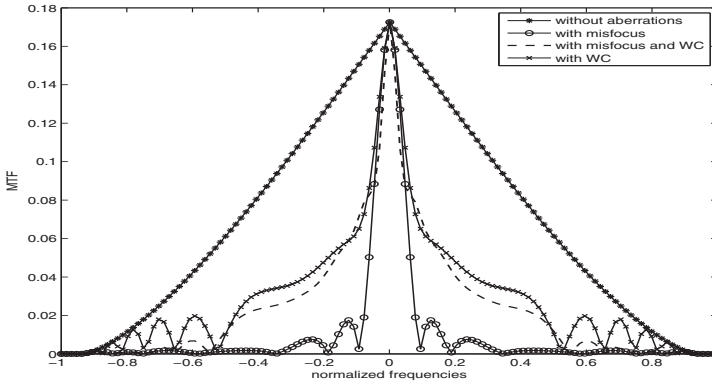


Fig. 7. Effect of different configurations of the imaging system on the MTF as a function of normalized frequencies (the maximum frequency equals one).

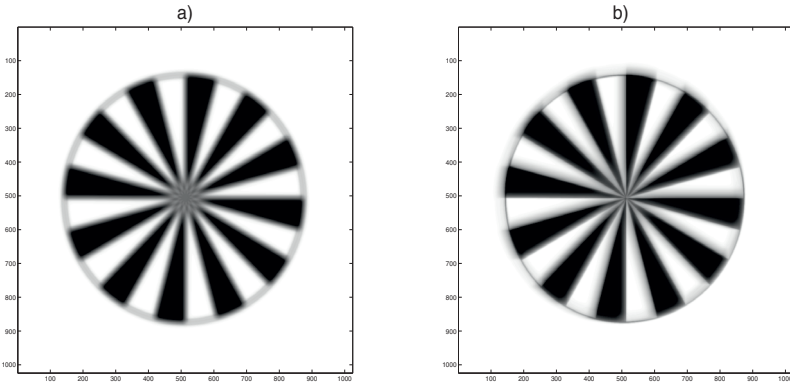


Fig. 8. Image observed in presence of a defocus with $\Psi_{\lambda_3} = 50$ without a) and with wavefront coding b). A cubic phase mask of the form 4.3 is considered with $\alpha = 116$.

4.2 Deconvolution of the images

The influence of the wavefront coding on the observed image is represented on Figures 8b and 9b. It clearly appears that the only introduction of a phase mask allows to reduce the blurring in the observation. The image obtained is then processed in order to still reduce the blurring effect. It is important to notice that the defocus default is not yet known. The deconvolution is thus done considering two configurations of the imaging system: a classical one, and another that introduces the wavefront coding. The results of the deconvolution are presented in Figures 10 and 11. The visual quality is still better when wavefront coding is used and is improved in comparison to the image of Figures 8b and 9b. In particular for the spoke pattern, the region in the center of the image is sharper and for the galaxy, the stars are closed to pointwise object.

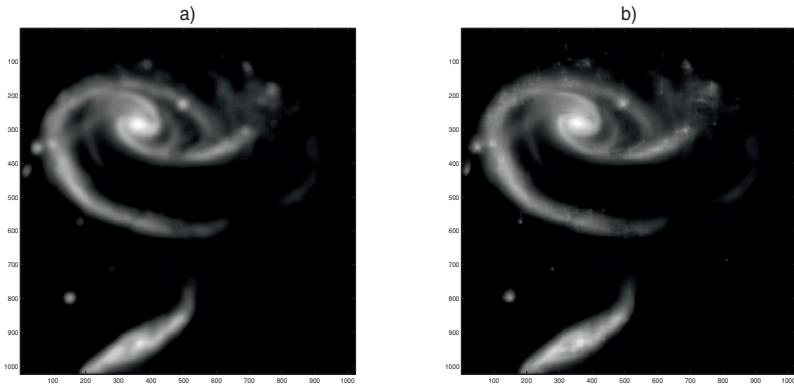


Fig. 9. Image observed in presence of a defocus with $\Psi_{\lambda_3} = 50$ without a) and with wavefront coding b). A cubic phase mask of the form 4.3 is considered with $\alpha = 119$.

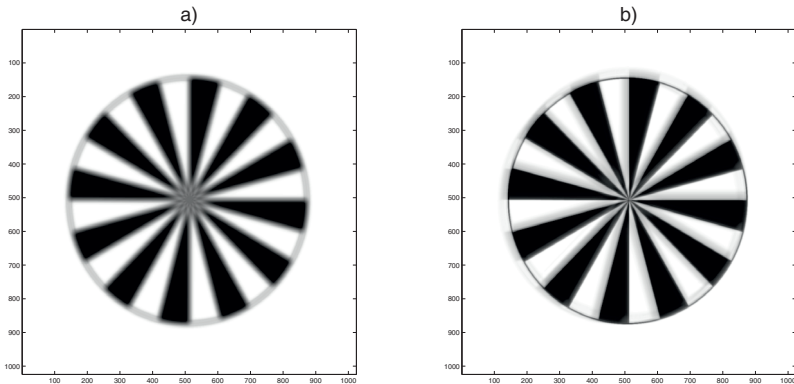


Fig. 10. Deconvolution of the image observed in presence of a defocus with $\Psi_{\lambda_3} = 50$ without a) and with wavefront coding b). A cubic phase mask of the form 4.3 is considered with $\alpha = 116$.

5 Optimization of the parameter of the cubic phase mask

The parameter α of the cubic phase mask must be optimized to obtain a efficient wavefront coding that corrects, after a processing step, the defocus default.

In the results presented in Figures 8b and 10b, the parameter α is chosen equal to 116. This parameter was obtained by considering a quality criterion on the reconstructed image. In our simulation, the chosen criterion is the Mean Square Error (MSE) between the true image of Figure 3a and the reconstructed image when wavefront coding is considered. Other choices of quality criterion can be done, for example the MSE can be averaged on several MSE (Diaz *et al.* 2010) obtained from different values of the defocus, leading to a phase mask robust to

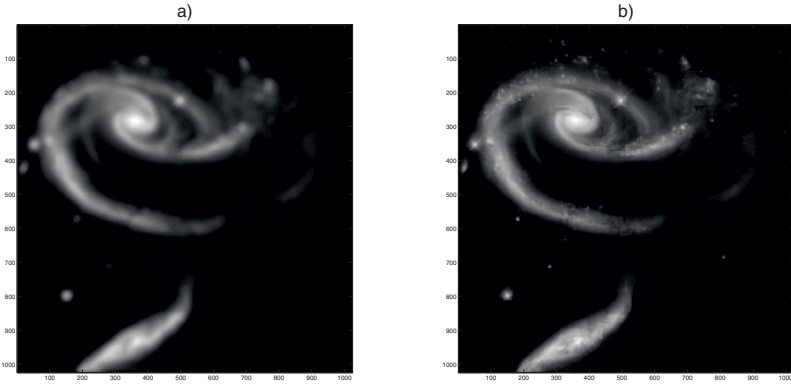


Fig. 11. Deconvolution of the image observed in presence of a defocus with $\Psi_{\lambda_3} = 50$ without a) and with wavefront coding b). A cubic phase mask of the form 4.3 is considered with $\alpha = 119$.

the defocus parameter. These criterions based on the calculus of the MSE can be considered only in simulations when the true object is known.

The MSE is represented in Figure 12 (curve c)) considering a parameter α varying between 1 and 200. The choice $\alpha = 116$ leads to the minimization of the mean square error when a defocus parameter of $\Psi_{\lambda_3} = 50$ is considered.

The curves of MSE obtained for different parameter of defocus (a) $\Psi_{\lambda_1} = 10$, b) $\Psi_{\lambda_2} = 20$) are also represented. It is clear that the value of the parameter α of the cubic mask depends on the defocus parameter, however the choice of α is not so sensitive to the defocus parameter. Indeed, a range of parameter α leads to similar values of the MSE. For example, for the defocus $\Psi_{\lambda_3} = 50$, α can be chosen in the range $[90, 170]$ without leading to significative degradation of the reconstruction.

For the image of the galaxy, the results presented in Figures 9b and 11b are obtained with a mask parameter $\alpha = 119$. The criterion used to optimize this value is still the MSE but computed over a small zone (100×100 pixels) of the image of Figure 4a. The use of the entire image of the galaxy gives a bad criterion of quality as the image is complex. The curves for the MSE in presence of different values of defocus are similar to the one of Figure 12 and are not represented.

6 Robustness of the cubic phase mask with respect to defocus

Once the parameter of the cubic phase mask is optimized, it is interesting to study its robustness with respect to defocus. The curve in Figure 13 represents the MSE between the reconstructed image and the true one when a cubic phase mask of parameter $\alpha = 116$ is chosen, and when the defocus parameter Ψ_{λ} varies from 0 (no defocus) to 150 (important defocus). The image considered is the spoke pattern represented in Figure 3a.

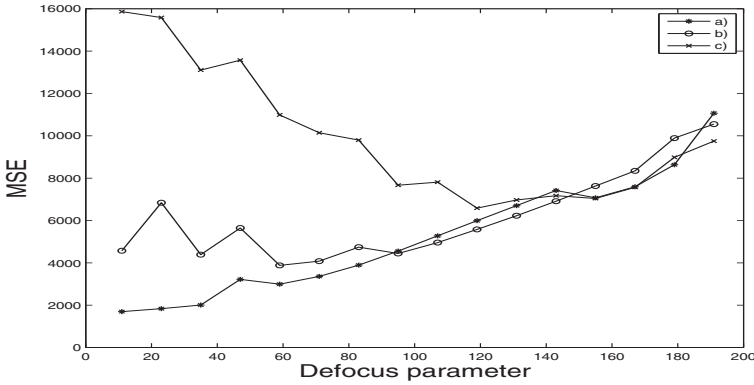


Fig. 12. Influence of the choice of the parameter α in the cubic phase mask for a fixed defocus a) $\Psi_{\lambda_1} = 10$, b) $\Psi_{\lambda_2} = 20$, c) $\Psi_{\lambda_3} = 50$.

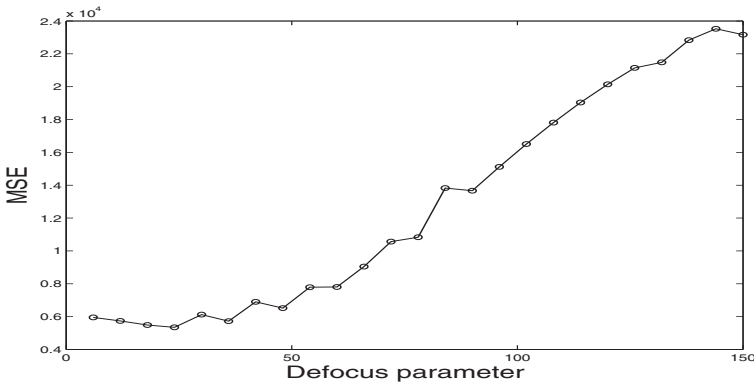


Fig. 13. Robustness of the optimization of the cubic phase mask towards defocus. The parameter α is taken equal to 116 which is the optimal value for a defocus parameter of $\Psi_{\lambda_3} = 50$ in the case of the spoke pattern.

It is clear that the parameter α depends on the defocus factor, however once the parameter α is fixed, similar results are obtained in term of MSE for a defocus parameter in $[0, 50]$. This result is illustrated on Figure 14 where the reconstructions b), d), f) are obtained with the same parameter ($\alpha = 116$) but considering respectively $\Psi_{\lambda_2} = 20$ (first line), $\Psi_{\lambda_3} = 50$ (second line), $\Psi_{\lambda_4} = 100$ (third line).

Once the phase mask is chosen, the optimization is a key point to obtain good quality results. However, the parameter α can take its value within a range allowing the imaging system to give good results when different values of defocus are introduced. It could be interesting for example when the defocus parameter is not constant over the whole pupil.

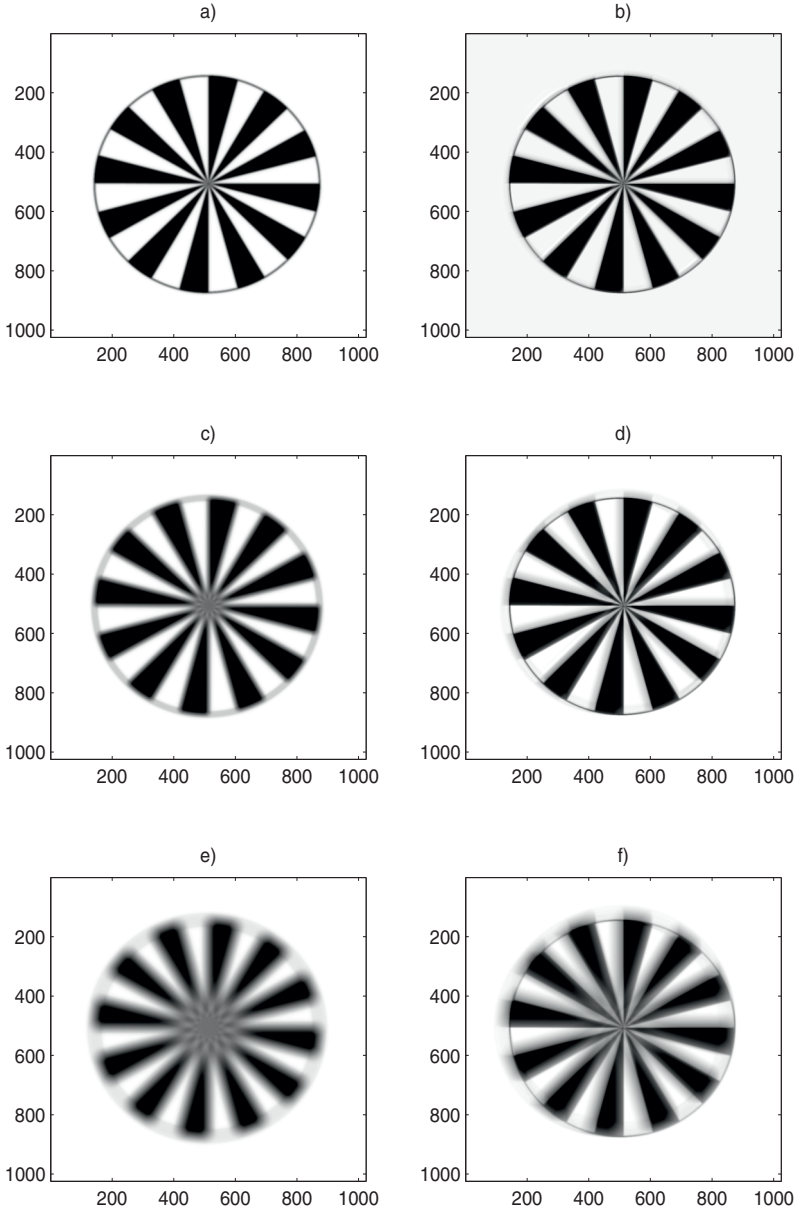


Fig. 14. Robustness of the optimization of the cubic phase mask towards defocus. Figures a), c), e) represent the degraded images with three different parameters of defocus $\Psi_{\lambda_2} = 20$, $\Psi_{\lambda_3} = 50$, $\Psi_{\lambda_4} = 100$. Figures b), d), f) represent the deconvolved images when a cubic phase mask of parameter $\alpha = 116$ is considered.

7 Conclusion

The wavefront coding is a technique that allows one, by introducing a pupil mask, to make insensitive the imaging system to some classical aberrations like defocus leading to increase the depth of field.

The use of wavefront coding, or other techniques that introduce the processing of the images jointly with the optics for the design of the imaging system, is going to increase in the following year. The reduction of the cost of the imaging system associated with the simplification of the conception, leading to high quality images after processing, make the hybrid imaging system of great interest.

The introduction of joint conception of optics and processing will introduce challenging tasks in next years to imagine or associate methods, to define new criterion to qualify the objective to reach, by adapting them to the target application.

References

- Arnison, M.R., Cogswell, C.J., Sheppard, C.J.R., & P., Török, 2007, *Optical Imaging Micros. Opt. Sci.*, 87, 169
- Caron, N., & Sheng, Y., 2008, *Appl. Opt.*, 47, E39
- Castro, A., & Ojeda-Castaneda, J., 2004, *Appl. Opt.*, 43, 3474
- Diaz, F., Goudail, F., Loiseaux, B., & Huignard, J.-P., 2009, *Opt. Lett.*, 34, 2970
- Diaz, F., Goudail, F., Loiseaux, B., & Huignard, J.-P., 2010, *J. Opt. Soc. Am. A*, 2123
- Dowski, E.R., Jr., & Cathey, A.T., 1995, *Appl. Opt.*, 34, 1859
- Cathey, W.T., & Dowski, E.R., 2002, *Appl. Opt.*, 41, 6080
- Goodman, J.W., 2005, *Fourier Optics*, Chapter 6 (Roberts and Company Publishers), 129
- Kubala, K.S., Dowski, E., Kobus, J., & Brown, R., 2004, *Proc. SPIE*, 5524, *Novel Optical Systems Design and Optimization VII*, 54
- Muyo, G., & Harvey, A.R., 2004, *Proc. SPIE*, 5612, 227
- Narayanswamy, R., Johnson, G.E., Silveira, P.E.X., *et al.*, 2004, *Appl. Opt.*, 44, 701
- Neil, M.A.A., Kuskaitis, R., Wilson, T., & Laczik, Z.J., 2000, *Opt. Lett.*, 25, 245
- Prasad, S., Torgersen, T.C., Pauca, V.P., Plemmons, R.J., & van der Gracht, J., 2004, *International Journal of Imaging Systems and Technology Special Issue: High-Resolution Image Reconstruction*, 14, 6774
- Sauceda, A., & Ojeda-Castaeda, J., 2004, *Opt. Lett.*, 29, 560
- Sherif, S., Cathey, T., & Dowski, E., 2004, *Appl. Opt.*, 43, 2709
- Wach, H.B., Dowski, E.R., & Cathey, W.T., 1998, *Appl. Opt.*, 37, 5359
- Yang, Q., Liu, L., & Sun, J., 2007, *Opt. Comm.*, 272, 56
- Zhao, H., Li, Q., & Feng, H., 2008, *Opt. Lett.*, 33, 1171